

# Optimal Gyricity Distribution for Space Structure Vibration Control

Stephen A. Chee\*

*McGill University, Montreal, Quebec H3A 0C3, Canada*

and

Christopher J. Damaren†

*University of Toronto, Toronto, Ontario M3H 5T6, Canada*

DOI: 10.2514/1.G000293

Many space vehicles have been launched with large flexible components such as booms and solar arrays. These large space structures may require active shape control given the possibility of lightly damped vibrations. Such vibrations can be controlled using a collection of control moment gyros, which consist of a spinning wheel in gimbals and produce a torque when the orientation of the wheel is changed. This study investigates the optimal distribution of these control moment gyros on large space structures for vibration suppression. Initially, a continuum model is adopted that represents the distribution of control moment gyros by a continuous distribution of stored angular momentum (gyricity). The optimal control solution for the gimbal motions (for a given gyricity distribution) is then optimized with respect to the gyricity distribution. Further investigation considers discrete parameter models of beam and a plate structures with evenly placed discrete pointwise control moment gyros. Numerical optimization of a suitable cost function allocates the amount of stored angular momentum possessed by these control moment gyros.

## I. Introduction

CONTROL moment gyros (CMGs) consist of a spinning rotor that is mounted in gimbals. Gimbal motion leads to gyroscopic reaction torques on the structure to which the CMG is attached. These torques are a linear function of the gimbal rates and can be used for spacecraft actuation. In addition, the mere presence of a CMG will lead to gyroscopic torques when the CMG experiences an angular velocity that is not parallel to the rotor spin axis. A single-gimbaled CMG (SGCMG) consists of a single gimbal axis and results in an output torque that is perpendicular to the spin and gimbal axes. A double-gimbaled CMG (DGCMG) consists of two gimbal axes and can be used to produce torques about two output axes. In a variable-speed CMG, the rotor spin rate is variable, which leads to a third output torque about the spin axis.

CMGs have been a popular choice for attitude control actuators for larger spacecraft and have been used on Skylab, Mir, and the International Space Station. There have been a few studies that have advocated their use as actuators to provide active damping on large flexible space structures. Aubrun and Margulies [1] introduced the concept of the gyrodamper. It consisted of an SGCMG with an angular rate sensor that measured the inertial angular rate about the output torque axis. They noted that the use of a constant proportional gain between the angular rate and the gimbal rate (hence, output torque) would mimic a purely passive rotational dashpot. They also provided the suggestion that two such devices could be mounted back-to-back so that the angular momentum bias they contributed would be nominally zero but, with gearing of the gimbal axes (in opposite directions), the output torques would reinforce one another. Such devices were termed scissored pairs in [2], where it was demonstrated that they could reduce power consumption.

An SGCMG gyrodamper prototype was constructed in [3] and mounted to the free end of a cantilevered beam, and active damping of

the flexural motions was demonstrated. A DGCMG prototype was attached to the tip of a slender cantilevered beam in [4], and a comparison of a double-gimbaled format to a single-gimbaled format was made to evaluate vibration suppression effectiveness. The DGCMG outperformed the SGCMG where it is noted that the latter relies on gyroscopic coupling to control vibration in two planes using a single gimbal. Simple adaptive control was used in [5] and applied to vibration control of flexible beam and plate structures using discrete pointwise control moment gyros. Optimal location of a single CMG, which could be used for slewing and vibration control of a truss-like beam, was explored in [6].

The possibility of locating potentially large numbers of spinning rotors on a flexible structure led D'Eleuterio and Hughes [7,8] to develop the notion of a gyroelastic continuum. They envisaged an elastic structure containing a continuous distribution of stored angular momentum parameterized by the gyricity distribution, the density of stored angular momentum per unit volume, which could vary throughout the structure. The basic partial differential equation model governing the motion of a gyroelastic continuum was developed in [7]. This was extended to the modeling of a distribution of CMGs by Damaren and D'Eleuterio [9] who posed and solved an optimal control problem for this class of space structures. They developed controllability conditions for a continuous or discrete distribution of CMGs in [10].

One stone left unturned in [9,10] was the determination of an optimal gyricity distribution, which can be thought of as the solution of the optimal actuator location problem for vibration control of a flexible structure using CMGs. The gyricity distribution is an ideal approach to this problem because it gives size and location information for a distribution of CMGs in the guise of a single function. The approximate implementation of a continuous distribution of CMGs as a discrete system of pointwise actuators was explored in [9] (for a plate) and [10] (for a beam).

The optimal location problem for CMGs is complexified by the fact that the open-loop dynamics are impacted by the amount and location of the stored angular momentum contributed by these devices. For example, the natural vibration frequencies are a function of the CMG distribution. An interesting question is whether it is better to have a single large CMG at a prescribed location (say at the tip of a beam), which presents a large stored angular momentum bias, or whether it is better to employ a distribution of many small devices implemented as scissored pairs, which contribute no stored angular momentum bias on average (nominally).

Received 27 September 2013; revision received 22 January 2014; accepted for publication 19 August 2014; published online 25 November 2014. Copyright © 2014 by Stephen Chee and Christopher Damaren. Published by the American Institute of Aeronautics and Astronautics, Inc., with permission. Copies of this paper may be made for personal or internal use, on condition that the copier pay the \$10.00 per-copy fee to the Copyright Clearance Center, Inc., 222 Rosewood Drive, Danvers, MA 01923; include the code 1533-3884/14 and \$10.00 in correspondence with the CCC.

\*Doctoral Candidate, Department of Mechanical Engineering. Student Member AIAA.

†Professor, Institute for Aerospace Studies. Associate Fellow AIAA.

In this paper, the problem of determining an optimal gyricity distribution will be formulated. This is the one that minimizes the value of a performance index that has already been minimized (with respect to gimbal motion) for a given gyricity distribution (i.e., “the minimum of a minimum” is sought). This will lead us to a condition that effectively maximizes the controllability of a given set of actuator locations. This condition is evaluated for simple gyroelastic beam and plate structures, which can be thought of as equivalent continuum models for large truss-like space structures. This analysis uses a continuous gyricity distribution but will be validated by optimizing the location of a discrete pointwise distribution using numerical optimization tools in conjunction with a discrete parameter representation of the structural dynamics.

Other researchers have advocated the use of film-type sensors and actuators for vibration control in the form of piezoelectric patches. Applications to space structure problems are described in [11–16]. From these works, it is clear that the control influences provided are small and suitable for suppressing low levels of vibration. They are also more applicable to continuous beam and plate structures than large-scale beam and plate structures whose underlying structure is truss-like. CMGs are capable of providing larger control influences in the form of torques, which can also be harnessed for attitude control. The optimal location of piezoelectric actuators is described in [17–19] for beams, plates, and spacecraft box structures, respectively.

## II. CMG Control of Gyroelastic Space Structures

The basic partial differential equation model governing the motion of a gyroelastic continuum was advanced in [7] and extended to the modeling of a distribution of CMGs in [9]. The basic vehicle  $V$  is depicted in Fig. 1 and consists of a rigid body  $R$  to which a number of flexible appendages, collectively denoted by  $E$ , are attached. Let  $\mathbf{w}(\mathbf{r}, t)$  denote the total displacement of the vehicle at position  $\mathbf{r} = [x \ y \ z]^T$  whose origin  $O$  lies on a (possibly vanishingly small) rigid portion  $R$  of the structure  $V$ . It can be decomposed into rigid-body and elastic deformations as follows:

$$\mathbf{w}(\mathbf{r}, t) = \mathbf{w}_0(t) - \mathbf{r} \times \boldsymbol{\theta}(t) + \mathbf{u}_e(\mathbf{r}, t) \quad (1)$$

Here,  $\mathbf{w}_0(t)$  is the translation of  $O$ ,  $\boldsymbol{\theta}(t)$  is the small rotation of  $R$ , and  $\mathbf{u}_e(\mathbf{r}, t)$  is the small elastic deformation, at position  $\mathbf{r}$ , with  $\mathbf{u}_e$  vanishing on  $R$ . The notation  $(\cdot)^\times$  implements the vector cross product:

$$\mathbf{r}^\times = \begin{bmatrix} 0 & -z & y \\ z & 0 & -x \\ -y & x & 0 \end{bmatrix}$$

The structure is imbued with a (nominal) gyricity distribution  $\mathbf{h}_s(\mathbf{r})$  (the stored angular momentum per unit volume) and it will be assumed that  $\mathbf{h}_s(\mathbf{r})$  vanishes on  $\partial V$ , the boundary of  $V$ .

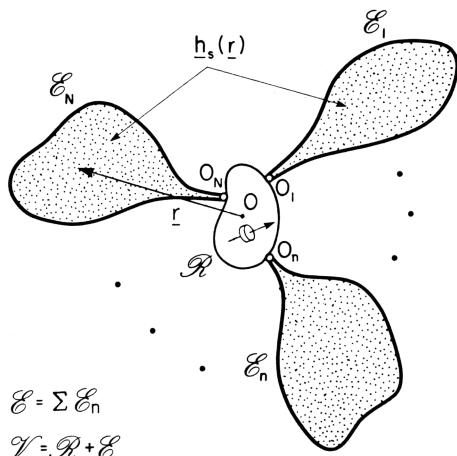


Fig. 1 Gyroelastic space structure.

It is assumed that the gyricity element at  $\mathbf{r}$ ,  $\mathbf{h}_s(\mathbf{r})dV$  can be rotated relative to the local body-fixed reference frame through small gimbal angles  $\boldsymbol{\beta}(\mathbf{r}, t) = [\beta_x \ \beta_y \ \beta_z]^T$ ,  $\|\boldsymbol{\beta}\| \ll 1$ . The model governing the dynamics of this flexible structure carrying a distribution of DGCMGs is given by [7,9,10]:

$$\mathcal{M}\ddot{\mathbf{w}} + (\mathcal{G} + \mathcal{D})\dot{\mathbf{w}} + \mathcal{K}\mathbf{w} = \mathcal{H}\mathbf{u} \quad (2)$$

where  $\mathcal{M} = \sigma(\mathbf{r})\mathcal{I}$  is the self-adjoint mass operator [with  $\sigma(\mathbf{r})$  the mass density per volume and  $\mathcal{I}$  the identity operator],  $\mathcal{K}$  is the self-adjoint stiffness operator, and  $\mathcal{D}$  is the self-adjoint damping operator. The stiffness and damping operators are positive definite with respect to  $\mathbf{u}_e$  and the mass operator is positive definite with respect to  $\mathbf{w}$ . The terms associated with the gyricity distribution are the gyricity operator  $\mathcal{G}$  and the input operator  $\mathcal{H}$ , defined by

$$\mathcal{G} = -\frac{1}{4}\nabla^\times \mathbf{h}_s^\times \nabla^\times, \quad \mathcal{H} = \frac{1}{2}\nabla^\times \mathbf{h}_s^\times \quad (3)$$

and the control input is  $\mathbf{u}(\mathbf{r}, t) = \dot{\boldsymbol{\beta}}(\mathbf{r}, t)$ , the gimbal rates, which are also assumed to be small. Hence, the force distribution created by the DGCMGs is

$$\mathbf{f}_h(\mathbf{r}, t) = -\mathcal{G}\dot{\mathbf{w}} + \mathcal{H}\mathbf{u} = \frac{1}{2}\nabla^\times \left\{ \mathbf{h}_s^\times(\mathbf{r}) \left[ \frac{1}{2}\nabla^\times \dot{\mathbf{w}}(\mathbf{r}, t) + \dot{\boldsymbol{\beta}}(\mathbf{r}, t) \right] \right\}$$

where the second  $1/2\nabla^\times$  operator produces an angular velocity distribution from the linear velocity distribution  $\dot{\mathbf{w}}(\mathbf{r}, t)$  and the first one produces a force distribution from a torque distribution.

The gyricity operator is skew adjoint, whereas the input operator is neither self-adjoint or skew adjoint. The skew-adjoint property of  $\mathcal{G}$  follows from the following form of integration by parts:

$$\int_V \mathbf{u}^T \nabla^\times \mathbf{v} dV = \int_V (\nabla^\times \mathbf{u})^T \mathbf{v} dV$$

if  $\mathbf{u}$  or  $\mathbf{v}$  vanishes on the boundary of  $V$ . It will be useful to introduce the inner product

$$\langle \mathbf{u}, \mathbf{v} \rangle = \int_V \mathbf{u}^T \mathbf{v} dV$$

Using this to define the adjoint of  $\mathcal{H}$  according to  $\langle \mathbf{u}, \mathcal{H}\mathbf{v} \rangle = \langle (\mathcal{H}^* \mathbf{u}), \mathbf{v} \rangle$ , one arrives at  $\mathcal{H}^* = -1/2\mathbf{h}_s^\times \nabla^\times$ .

It will be helpful to express Eq. (1) in first-order form:

$$\mathcal{E}\dot{\boldsymbol{\chi}} + \mathcal{T}\boldsymbol{\chi} = \mathcal{B}\mathbf{u} \quad (4)$$

where

$$\mathcal{E} = \begin{bmatrix} \mathcal{M} & 0 \\ 0 & \mathcal{K} \end{bmatrix}, \quad \mathcal{T} = \begin{bmatrix} \mathcal{G} + \mathcal{D} & \mathcal{K} \\ -\mathcal{K} & 0 \end{bmatrix},$$

$$\mathcal{B} = \begin{bmatrix} \mathcal{H} \\ 0 \end{bmatrix}, \quad \boldsymbol{\chi} = \begin{bmatrix} \dot{\mathbf{w}} \\ \mathbf{u}_e \end{bmatrix}$$

The second equation contained in Eq. (4) states that  $\mathcal{K}\dot{\mathbf{u}}_e = \mathcal{K}\dot{\mathbf{w}}$ , which holds by virtue of the fact that the rigid part of the motion lies in the null space of the stiffness operator  $\mathcal{K}$ . Using the inner product, the operator  $\mathcal{E}$  is self-adjoint and positive definite:

$$\langle \boldsymbol{\chi}_1, \mathcal{E}\boldsymbol{\chi}_2 \rangle = \langle \mathcal{E}\boldsymbol{\chi}_1, \boldsymbol{\chi}_2 \rangle, \quad \langle \boldsymbol{\chi}, \mathcal{E}\boldsymbol{\chi} \rangle > 0 (\boldsymbol{\chi} \neq 0)$$

The operator  $\mathcal{T}$  can be decomposed into skew-adjoint and self-adjoint parts:

$$\mathcal{T} = \mathcal{S} + \delta\mathcal{S}$$

where

$$\mathcal{S} = \begin{bmatrix} \mathcal{G} & \mathcal{K} \\ -\mathcal{K} & 0 \end{bmatrix}, \quad \delta\mathcal{S} = \begin{bmatrix} \mathcal{D} & 0 \\ 0 & 0 \end{bmatrix}$$

The notation has been chosen to suggest that damping will be treated as a small perturbation.

### A. Eigenvalue Problem

The eigenvalue problem associated with the undamped and unforced form of Eq. (4) is given by

$$\lambda_\alpha \mathcal{E} \chi_\alpha + \mathcal{S} \chi_\alpha = 0 \quad (5)$$

Given the properties of  $\mathcal{E}$  and  $\mathcal{S}$ , it is easily shown that the eigenvalues  $\lambda_\alpha$  are purely imaginary and the eigenfunctions occur in complex-conjugate pairs:

$$\lambda_\alpha = j\omega_\alpha, \quad \chi_\alpha = \phi_\alpha + j\psi_\alpha \quad (\alpha = -\infty, \dots, \infty) \quad (6)$$

where  $\omega_{-\alpha} = -\omega_\alpha$ ,  $\omega_\alpha > 0$  for  $\alpha > 0$ , and  $\phi_{-\alpha} = \psi_\alpha$ . There are also zero-frequency modes, which will not concern us here. The real eigenfunctions have the following forms:

$$\phi_\alpha = \begin{bmatrix} -\omega_\alpha \mathbf{v}_\alpha \\ \mathbf{u}_{e\alpha} \end{bmatrix}, \quad \psi_\alpha = \begin{bmatrix} \omega_\alpha \mathbf{u}_\alpha \\ \mathbf{v}_{e\alpha} \end{bmatrix}$$

where  $\mathbf{u}_{-\alpha} = \mathbf{v}_\alpha$ ,  $\mathbf{u}_{e,-\alpha} = \mathbf{v}_{e\alpha}$ , and

$$\mathbf{u}_\alpha = \mathbf{w}_{0\alpha} - \mathbf{r}^\times \theta_\alpha + \mathbf{u}_{e\alpha}$$

which partitions the mode shape according to Eq. (1). A perturbation analysis for the eigenvalues reveals that the perturbation  $\delta\mathcal{S}$  leads to changes in the eigenvalues given by

$$\delta\lambda_\alpha = -\frac{1}{4\omega_\alpha^2} \langle \chi_\alpha, \delta\mathcal{S} \chi_\alpha \rangle = -\frac{1}{4} [\langle \mathbf{u}_\alpha, \mathcal{D} \mathbf{u}_\alpha \rangle + \langle \mathbf{v}_\alpha, \mathcal{D} \mathbf{v}_\alpha \rangle] \quad (7)$$

Hence, the damping perturbation leads to negative real changes in the eigenvalues as expected. The first relation in Eq. (7) is also valid for the case where  $\mathcal{G}$  is taken to be zero in  $\mathcal{S}$ , and  $\mathcal{D}$  is set equal to  $\mathcal{G}$  in  $\delta\mathcal{S}$ . In this situation, gyricity is viewed as a small perturbation to a purely elastic undamped system. Because  $\mathcal{G}$  is skew adjoint, we arrive at

$$\delta\lambda_\alpha = \frac{j}{2\omega_\alpha^2} \langle \psi_\alpha, \delta\mathcal{S} \phi_\alpha \rangle = j\delta\omega_\alpha, \quad \delta\omega_\alpha = -\frac{1}{2} \langle \mathbf{u}_\alpha, \mathcal{G} \mathbf{v}_\alpha \rangle$$

For a purely elastic system, one can select  $\mathbf{u}_\alpha = \mathbf{v}_\alpha$ , which, using the skew-adjoint property of  $\mathcal{G}$ , leads to  $\delta\omega_\alpha = 0$ . Hence, the first-order change in vibration frequencies due to gyricity is zero.

### B. Continuum Optimal Control Problem

For a given gyricity distribution, the optimal control law for the gimbal rates is that which minimizes the performance index

$$\mathcal{J}[\mathbf{u}] = \frac{1}{2} \int_0^T [\langle \chi, \mathcal{Q} \chi \rangle + \langle \mathbf{u}, \mathcal{R} \mathbf{u} \rangle] dt \quad (8)$$

where  $\mathcal{R} = \mathbf{R}(\mathbf{r})\mathcal{I}$  is a positive-definite self-adjoint operator [with the matrix  $\mathbf{R}(\mathbf{r})$  being positive definite] and  $\mathcal{Q}$  is a positive-semidefinite self-adjoint operator. It is assumed that does not penalize the translational modes of the system. It was shown in [9] that the optimal control law is given by

$$\mathbf{u}(\mathbf{h}_s) = -\mathcal{R}^{-1} \mathcal{B}^*(\mathbf{h}_s) \xi(\mathbf{h}_s) \quad (9)$$

where the adjoint state  $\xi$  is part of the solution of the following two-point boundary value problem:

$$\mathcal{E} \dot{\chi}(\mathbf{h}_s) + \mathcal{T}(\mathbf{h}_s) \chi(\mathbf{h}_s) = -\mathcal{W}(\mathbf{h}_s) \xi(\mathbf{h}_s), \quad \chi(\mathbf{h}_s)|_{t=0} = \chi_0 \quad (10)$$

$$-\mathcal{E} \dot{\xi}(\mathbf{h}_s) + \mathcal{T}^*(\mathbf{h}_s) \xi(\mathbf{h}_s) = \mathcal{Q} \chi(\mathbf{h}_s), \quad \xi(\mathbf{h}_s)|_{t=T} = 0 \quad (11)$$

where  $\mathcal{W}(\mathbf{h}_s) = \mathcal{B}(\mathbf{h}_s) \mathcal{R}^{-1} \mathcal{B}^*(\mathbf{h}_s)$ . The functional dependence on  $\mathbf{h}_s$  in Eqs. (9–11) is used to exhibit either explicit or implicit dependence on the gyricity distribution and anticipates the need to vary it.

The ‘‘sweep solution’’  $\xi(\mathbf{h}_s) = \mathcal{P}(\mathbf{h}_s) \mathcal{E} \chi(\mathbf{h}_s)$  leads to the operator Riccati equation for  $\mathcal{P}$ :

$$\mathcal{E} \dot{\mathcal{P}} \mathcal{E} = \mathcal{E} \mathcal{P} \mathcal{T} + \mathcal{T}^* \mathcal{P} \mathcal{E} + \mathcal{E} \mathcal{P} \mathcal{B} \mathcal{R}^{-1} \mathcal{P} \mathcal{E} - \mathcal{Q} \quad (12)$$

with terminal boundary condition  $\mathcal{P}|_{t=T} = 0$ . The optimal value of the performance index is

$$\mathcal{J}(\mathbf{h}_s) \triangleq \mathcal{J}[\mathbf{u}(\mathbf{h}_s)] = \frac{1}{2} \langle \chi(\mathbf{h}_s), \mathcal{E} \mathcal{P}(\mathbf{h}_s) \mathcal{E} \chi(\mathbf{h}_s) \rangle|_{t=0} \quad (13)$$

A modal expansion approach for the Riccati operator  $\mathcal{P}$  and the motion of the structure  $\chi$  described by Eq. (4) was adopted in [9] to calculate the solution to the optimal control problem, the motion it produced, and the value of the optimal cost.

It is interesting to note how the optimal value (for a given  $\mathbf{h}_s$ ) varies with respect to  $\mathbf{h}_s$ . To this end, introduce a neighboring gyricity distribution  $\mathbf{h}_s^*$  and define

$$\gamma = \chi(\mathbf{h}_s^*) - \chi(\mathbf{h}_s) \quad (14)$$

$$\delta = \xi(\mathbf{h}_s^*) - \xi(\mathbf{h}_s) \quad (15)$$

$$\delta\mathcal{T} = \mathcal{T}(\mathbf{h}_s^*) - \mathcal{T}(\mathbf{h}_s) = \begin{bmatrix} \mathcal{G}(\mathbf{h}_s^*) - \mathcal{G}(\mathbf{h}_s) & 0 \\ 0 & 0 \end{bmatrix}$$

$$\gamma_0 = \chi(\mathbf{h}_s^*)|_{t=0} - \chi(\mathbf{h}_s)|_{t=0} = 0$$

$$\delta_T = \xi(\mathbf{h}_s^*)|_{t=T} - \xi(\mathbf{h}_s)|_{t=T} = 0$$

$$\delta_0 = \xi(\mathbf{h}_s^*)|_{t=0} - \xi(\mathbf{h}_s)|_{t=0} \quad (16)$$

$$= [\mathcal{P}(\mathbf{h}_s^*)|_{t=0} - \mathcal{P}(\mathbf{h}_s)|_{t=0}] \mathcal{E} \chi_0, \quad \chi_0 = \chi|_{t=0} \quad (17)$$

It is demonstrated in the Appendix that

$$\begin{aligned} \mathcal{J}(\mathbf{h}_s) - \mathcal{J}(\mathbf{h}_s^*) &= \frac{1}{2} \int_0^T \langle \xi(\mathbf{h}_s^*), [\mathcal{W}(\mathbf{h}_s^*) - \mathcal{W}(\mathbf{h}_s)] \xi(\mathbf{h}_s^*) \rangle dt \\ &+ \int_0^T \langle \xi(\mathbf{h}_s^*), \delta\mathcal{T} \chi(\mathbf{h}_s) \rangle dt + \frac{1}{2} \int_0^T [\langle \delta, \mathcal{W}(\mathbf{h}_s) \delta \rangle + \langle \gamma, \mathcal{Q} \gamma \rangle] dt \end{aligned} \quad (18)$$

This expression provides an ideal starting for optimizing the gyricity distribution.

### III. Toward an Optimal Gyricity Distribution

A general problem that can be posed is as follows: Find  $\mathbf{h}_s^*$  such that

$$\mathcal{J}(\mathbf{h}_s^*) \leq \mathcal{J}(\mathbf{h}_s), \quad \forall \mathbf{h}_s \in H_{\text{ad}} \quad (19)$$

where  $H_{\text{ad}}$  is an admissible set of gyricity distributions:

$$H_{\text{ad}} = \{\mathbf{h}_s | \mathbf{h}_s(\mathbf{r}) = 0, \mathbf{r} \in \partial V, \|\mathbf{h}_s\| = H\} \quad (20)$$

and

$$\|\mathbf{h}_s\|^2 = \int_V \mathbf{h}_s^T \mathbf{h}_s dV$$

In general, an analytical solution to this problem is not possible. However, a sufficient condition for  $\mathbf{h}_s^*$  to be optimal can be obtained

from Eq. (18). Because  $\mathcal{W}$  and  $\mathcal{Q}$  are positive semidefinite, the following statement must hold: If

$$\frac{1}{2} \int_0^T \langle \xi(\mathbf{h}_s^*), [\mathcal{W}(\mathbf{h}_s^*) - \mathcal{W}(\mathbf{h}_s)] \xi(\mathbf{h}_s^*) \rangle dt + \int_0^T \langle \xi(\mathbf{h}_s^*), \delta \mathcal{T} \chi(\mathbf{h}_s) \rangle dt \geq 0 \quad (21)$$

then  $\mathcal{J}(\mathbf{h}_s^*) \leq \mathcal{J}(\mathbf{h}_s)$ . Proceeding heuristically, let us ignore the influence of gyricity on the open-loop dynamics  $\delta \mathcal{T} \approx 0$ . This is reasonable because, as noted earlier, the first-order change in the vibration frequencies due to gyricity is zero.

The minimization of the performance index clearly depends on maximizing the size of the positive-semidefinite operator  $\mathcal{W}$  where

$$\mathcal{W} = \begin{bmatrix} \mathcal{H} \mathcal{R}^{-1} \mathcal{H}^* & 0 \\ 0 & 0 \end{bmatrix}, \quad \mathcal{H} \mathcal{R}^{-1} \mathcal{H}^* = -\frac{1}{4} \nabla \times \mathbf{h}_s^* \mathcal{R}^{-1} \mathbf{h}_s^* \nabla \times \quad (22)$$

Letting  $\mathcal{R} = \mathcal{I}$ , maximizing the size of  $\mathcal{W}$  is equivalent to maximizing the size of  $\mathcal{H} \mathcal{H}^*$ . To this end, consider the quantities

$$S_{\alpha\alpha} = \langle \mathbf{u}_\alpha, \mathcal{H} \mathcal{H}^* \mathbf{u}_\alpha \rangle = -\frac{1}{4} \int_V (\nabla \times \mathbf{u}_\alpha)^T \mathbf{h}_s^* \mathbf{h}_s^* (\nabla \times \mathbf{u}_\alpha) dV \quad (23)$$

which were introduced in [10]. A proxy for maximizing  $\mathcal{W}$  is maximizing the size of these quantities (the  $S_{\alpha\alpha}$ ). In [10], it was shown that  $S_{\alpha\alpha} \neq 0$  or  $S_{-\alpha, -\alpha} \neq 0$  were conditions for controllability of mode pair  $\alpha$  using a distribution of DGCMGs. Another interpretation is possible by considering the collocated control law  $\mathbf{u}(\mathbf{r}, t) = -r^{-1} \mathcal{H}^* \dot{\mathbf{w}}(\mathbf{r}, t) = (2r)^{-1} \mathbf{h}_s^*(\mathbf{r}) \nabla \times \dot{\mathbf{w}}(\mathbf{r}, t)$ , which is a distributed DGCMG implementation of the gyrodamper introduced in [1]. Using the eigenperturbation formula from Eq. (7) with  $\mathcal{D} = r^{-1} \mathcal{H} \mathcal{H}^* = -(4r)^{-1} \nabla \times \mathbf{h}_s^* \mathbf{h}_s^* \nabla \times$ , the eigenvalue perturbations for large  $r$  are given by

$$\delta \lambda_\alpha = -\frac{1}{4r} (S_{\alpha\alpha} + S_{-\alpha, -\alpha}), \quad \alpha = 1, 2, 3, \dots \quad (24)$$

Clearly, it is desirable to maximize the magnitude of these quantities, which maximizes the controllability of mode pair  $\alpha$ . The fundamental problem is the dependence of the mode shapes  $\mathbf{u}_\alpha$  (and hence  $S_{\alpha\alpha}$ ) on the gyricity distribution, which is the quantity to be optimized.

In [20], the stored angular momentum coefficients are defined as

$$\mathbf{g}_\alpha = -\frac{1}{2} \int_V \mathbf{h}_s^* \nabla \times \mathbf{u}_\alpha dV \quad (25)$$

and shown to satisfy the modal identity

$$\begin{aligned} \frac{1}{2} \sum_{\alpha=-\infty}^{\infty} \mathbf{g}_\alpha \mathbf{g}_\alpha^T &= \frac{1}{4} \int_V (\nabla \times \mathbf{h}_s^*)^T (\nabla \times \mathbf{h}_s^*) \sigma^{-1} dV \\ &= -\frac{1}{4} \int_V \mathbf{h}_s^* \nabla \times \nabla \times \mathbf{h}_s^* \sigma^{-1} dV \end{aligned} \quad (26)$$

Using the Cauchy–Schwartz inequality, one can obtain the inequality

$$\mathbf{g}_\alpha^T \mathbf{g}_\alpha \leq \int_V dV \cdot S_{\alpha\alpha} \quad (27)$$

and combining these two equations yields

$$\begin{aligned} \frac{1}{2} \sum_{\alpha=-\infty}^{\infty} \mathbf{g}_\alpha^T \mathbf{g}_\alpha &= -\frac{1}{4} \text{tr} \int_V \mathbf{h}_s^* \nabla \times \nabla \times \mathbf{h}_s^* \sigma^{-1} dV \\ &= -\frac{1}{4} \int_V \mathbf{h}_s^T [\nabla \nabla^T + \nabla^T \nabla] \mathbf{h}_s \sigma^{-1} dV \\ &\leq \frac{V}{2} \sum_{\alpha=1}^{\infty} (S_{\alpha\alpha} + S_{-\alpha, -\alpha}) \end{aligned} \quad (28)$$

where  $\text{tr}$  denotes the trace of a square matrix. The second equality can be reasoned by direct expansion. The advantage of maximizing the lower bound established here is that it is independent of the mode shapes  $\mathbf{u}_\alpha$ , unlike the summation involving the  $S_{\alpha\alpha}$ . In other words, the limiting sum in the lower bound is independent of the modal parameters and depends only on the gyricity distribution and the mass density. Let us define this sum as

$$\begin{aligned} \mathcal{C}(\mathbf{h}_s) &\triangleq \frac{1}{2} \sum_{\alpha=-\infty}^{\infty} \mathbf{g}_\alpha^T \mathbf{g}_\alpha = \frac{1}{4} \int_V \mathbf{h}_s^T \mathcal{K}_h \mathbf{h}_s \sigma^{-1} dV, \\ \mathcal{K}_h &\triangleq -(\nabla \nabla^T + \nabla^T \nabla) \end{aligned} \quad (29)$$

The operator that has been defined as  $\mathcal{K}_h$  has the interesting interpretation of being the stiffness operator of a linear elastic, uniform, isotropic solid with Poisson's ratio equal to zero.

The gyricity distribution is now determined that produces stationary values of  $\mathcal{C}(\mathbf{h}_s)$  subject to the condition  $\mathbf{h}_s \in H_{\text{ad}}$ , that is,

$$\mathbf{h}_s(\mathbf{r}) = 0, \quad \mathbf{r} \in \partial V, \quad \|\mathbf{h}_s\| = H \quad (30)$$

This does not guarantee that the sum of the quantities  $S_{\alpha\alpha}$  [or  $\mathcal{J}(\mathbf{h}_s)$ ] will be stationary, but it does render stationary a lower bound for the sum on the right-hand side of the inequality in Eq. (28). With the boundary condition on  $\mathbf{h}_s$  in Eq. (30), the operator  $\mathcal{K}_h$  is rendered self-adjoint and positive definite. Application of the calculus of variations to the functional  $\mathcal{C}(\mathbf{h}_s)$  yields the following eigenproblem for the stationary values  $\mathcal{C}_m$  and the stationary distributions  $\mathbf{h}_m$ :

$$\begin{aligned} -\lambda_m \sigma(\mathbf{r}) \mathbf{h}_m + \mathcal{K}_h \mathbf{h}_m &= 0, \quad \int_V \mathbf{h}_m^T \mathbf{h}_m dV = H^2, \\ \mathcal{C}_m &= \frac{H^2 \lambda_m}{4}, \quad m = 1, 2, 3, \dots \end{aligned}$$

In general, the stationary values form an ascending sequence so that the maximum value of the index  $\mathcal{C}$  tends toward infinity.

As an example of the preceding, consider the beam example introduced in [10] and depicted in Fig. 2. This is a free–free beam that can bend in two planes and the gyricity distribution is nominally directed along the beam's slender axis. In this case, the operator  $\mathcal{K}_h$  degenerates to  $-2d^2/dx^2$  and the aforementioned eigenproblem is simply that of a uniform string with mass density per unit length  $\sigma = \rho$ . The stationary values and functions are given by

$$h_m = H \sqrt{\frac{2}{\ell}} \sin \frac{m\pi \hat{x}}{\ell}, \quad \left( \hat{x} = x + \frac{\ell}{2} \right), \quad \lambda_m = \frac{2}{\rho} (m\pi/\ell)^2$$

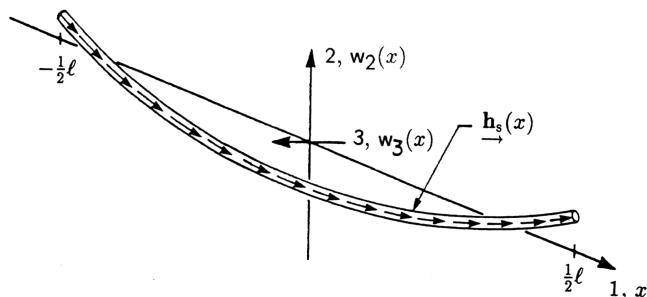


Fig. 2 Gyroelastic beam.

The stationary functions for the gyricity distribution have the property that, as  $m \rightarrow \infty$ , the average density of stored angular momentum on a nonzero, finite segment of the beam is zero. In this case, the CMGs behave like the scissored pairs considered in [2], which mount two CMGs back-to-back to cancel their nominal angular momentum but gear their gimbal motions together so that the control torques are reinforced. It was noted in the Introduction that a similar device was proposed in [1].

Let us now consider the plate example of [9], which treated the transverse motions of a free thin plate with the nominal gyricity distribution normal to the plate. If the origin is placed at the plate center, let  $x$  and  $y$  be the in-plane coordinate axes (with corresponding plate dimensions  $a$  and  $b$ ) and  $z$  normal to the plate. The stiffness operator is  $\mathcal{K} = D\nabla^4$  ( $D$  is the plate rigidity) and  $\mathcal{K}_h$  is that corresponding to a membrane with uniform tension. The stationary functions and values are

$$h_{mn} = \frac{2H}{\sqrt{ab}} \sin \frac{m\pi\hat{x}}{a} \sin \frac{n\pi\hat{y}}{b}, \quad \left( \hat{x} = x + \frac{a}{2}, \hat{y} = y + \frac{b}{2} \right),$$

$$\lambda_{mn} = \frac{1}{\sigma} [(m\pi/a)^2 + (n\pi/b)^2], \quad m, n = 1, 2, 3, \dots$$

Similar comments to the beam case apply here. Effectively, the gyroscopic terms emanating from the operator  $\mathcal{G}$  tend toward zero but those produced by  $\mathcal{H}\beta$  are maximized as  $m, n \rightarrow \infty$ . These results suggest that the angular moment bias contributed by the CMGs is not desirable and should be locally canceled by alternating the direction of the stored angular moment bias in neighboring CMGs.

## IV. Numerical Optimization

### A. Discrete Optimal Control Problem

Using a Ritz technique such as the finite element method, the partial differential equation in Eq. (2) can be spatially discretized to yield the discrete parameter model

$$\mathbf{M}\ddot{\mathbf{q}} + (\mathbf{G} + \mathbf{D})\dot{\mathbf{q}} + \mathbf{K}\mathbf{q} = \mathbf{H}\dot{\beta} \quad (31)$$

where  $\mathbf{q}(t)$  are the totality of the discrete parameters used to describe  $\mathbf{w}(\mathbf{r}, t)$  and  $\mathbf{M}$ ,  $\mathbf{G}$ ,  $\mathbf{D}$ ,  $\mathbf{K}$ , and  $\mathbf{H}$  are the constant matrices corresponding to their operator equivalents  $\mathcal{M}$ ,  $\mathcal{G}$ ,  $\mathcal{D}$ ,  $\mathcal{K}$ , and  $\mathcal{H}$ . It is assumed that the gyricity distribution corresponds to a set of  $N$  pointwise DGCMGs, that is,

where

$$\mathbf{Q}_{\text{rigid}} = \begin{cases} q, & \text{for diagonal positions corresponding to the rigid rotation states,} \\ 0, & \text{elsewhere} \end{cases}$$

Here,  $q$  is a positive constant chosen to place the eigenvalues of the closed-loop system matrix associated with the rigid modes.

$$\mathbf{h}_s(\mathbf{r}) = \sum_{i=1}^N \mathbf{h}_i \delta(\mathbf{r} - \mathbf{r}_i)$$

where  $\delta(\mathbf{r})$  is the Dirac delta function. The corresponding discrete set of gimbal angles will be denoted by  $\beta(t) = [\beta_{x1}, \beta_{y1}, \dots, \beta_{xN}, \beta_{yN}]^T$ . Equation (31) can be expressed in the following first-order state-space form:

$$\dot{\mathbf{x}} = \mathbf{A}\mathbf{x} + \mathbf{B}\mathbf{u}$$

where

$$\mathbf{A} = \begin{bmatrix} -\mathbf{M}^{-1}(\mathbf{G} + \mathbf{D}) & -\mathbf{M}^{-1}\mathbf{K} \\ \mathbf{1} & \mathbf{0} \end{bmatrix}, \quad \mathbf{B} = \begin{bmatrix} -\mathbf{M}^{-1}\mathbf{H} \\ \mathbf{0} \end{bmatrix},$$

$$\mathbf{x} = \begin{bmatrix} \dot{\mathbf{q}} \\ \mathbf{q} \end{bmatrix}, \quad \mathbf{u} = \dot{\beta}$$

In this section, a discrete linear quadratic regulator (LQR) control scheme is implemented. The optimal LQR controller yields a state feedback controller that minimizes the cost function

$$J = \int_0^{\infty} (\mathbf{x}^T \mathbf{Q} \mathbf{x} + \mathbf{u}^T \mathbf{R} \mathbf{u}) dt = \mathbf{x}_0^T \mathbf{P} \mathbf{x}_0 \quad (32)$$

(the factor of 1/2 is omitted in this section) where  $\mathbf{Q}$  is the positive-semidefinite matrix that penalizes the system's states,  $\mathbf{R}$  is a positive-definite matrix that penalizes the control inputs,  $\mathbf{P}$  is the solution to the algebraic Riccati equation

$$\mathbf{P}\mathbf{A} + \mathbf{A}^T\mathbf{P} - \mathbf{P}\mathbf{B}\mathbf{R}^{-1}\mathbf{B}^T\mathbf{P} + \mathbf{Q} = \mathbf{0}$$

and  $\mathbf{x}_0$  is the state of the system at time  $t = 0$ . The unique controller that minimizes  $J$  is of the form

$$\mathbf{u}(t) = -\mathbf{R}^{-1}\mathbf{B}^T\mathbf{P}\mathbf{x}(t)$$

Because the control objective is to suppress the vibrations of the system, it would seem appropriate to penalize the states  $\mathbf{x}$  according to the mechanical energy of the system. To this end, consider

$$\mathbf{Q} = \text{diag}\{\mathbf{M}, \mathbf{K}\}$$

which yields

$$\mathbf{x}^T \mathbf{Q} \mathbf{x} = \dot{\mathbf{q}}^T \mathbf{M} \dot{\mathbf{q}} + \mathbf{q}^T \mathbf{K} \mathbf{q}$$

It should be noted that, in the case of an unconstrained body, this choice of penalization does not penalize the rigid rotation of the structure. It penalizes only the rates of the rigid modes via  $\mathbf{M}$  because  $\mathbf{K}$  is only positive semidefinite. To penalize the rigid rotation of the structure,  $\mathbf{Q}$  is modified to be

$$\mathbf{Q} = \text{diag}\{\mathbf{M}, \mathbf{K}\} + \mathbf{Q}_{\text{rigid}} \quad (33)$$

To penalize the control effort, the matrix  $\mathbf{R}$  is chosen to have the form

$$\mathbf{R} = r\mathbf{1}$$

where  $r$  is a positive constant chosen to place the eigenvalues of the closed-loop system matrix. This effectively penalizes the gimbal rate motions uniformly.

### B. Optimization Objective

The objective of this analysis is to find the optimal distribution of CMGs for vibration suppression of beams and plates. A suitable objective function can be found in the objective function used for the optimal LQR problem shown in Eq. (32). In this equation, the initial state  $\mathbf{x}_0$  is unknown and can be considered as a random variable

**Table 1** Beam properties

Property	Symbol	Value
Beam length	$l$	100 m
Mass per length	$\rho$	6.200 kg/m
Stiffness to bending in two axis	$B_2$	$1.5765 \times 10^9 \text{ N} \cdot \text{m}^2$
Stiffness to bending in three axis	$B_3$	$1.5 \times B_2$
Proportional damping ratios	$\zeta_\alpha$	0.01
Rigid rotation penalization, Eq. (33)	$q$	100

with a second-order moment  $\mathcal{E}\{\mathbf{x}_0 \mathbf{x}_0^T\} = \mathbf{X}_0$ . From [21], it can be seen that minimizing  $J = \mathcal{E}\{\mathbf{x}_0^T \mathbf{P} \mathbf{x}_0\}$  is equivalent to minimizing  $J = \text{tr}(\mathbf{P} \mathbf{X}_0)$ ; assuming  $\mathbf{X}_0 = \mathbf{I}$ ,

$$J = \text{tr}(\mathbf{P})$$

is taken as the objective function. This makes the optimization a weighted sum of how quickly the vibrations are damped and the amount of control effort used.

Because both the location and amount of stored angular momentum influence the control of the structure in a coupled manner, the amount of stored angular momentum in each CMG is varied while keeping the locations of the CMGs fixed. This allows a fixed number of CMGs to be distributed evenly about the body, and the optimization will be concerned with the allocation of the stored angular momentum. Let  $\mathbf{h} = [h_{s,1}, h_{s,1}, \dots, h_{s,N}]^T$  be an array of the amount of nominal stored angular momentum for  $N$  CMGs. This distribution of stored angular momentum is subjected to the constraint

$$\sum_{k=1}^N h_{s,k}^2 = \mathbf{h}^T \mathbf{h} = c^2, \quad \text{or} \quad \bar{c}(\mathbf{h}) = \mathbf{h}^T \mathbf{h} - c^2 = 0$$

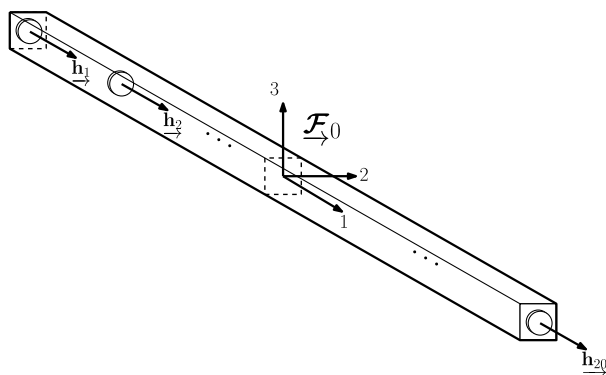
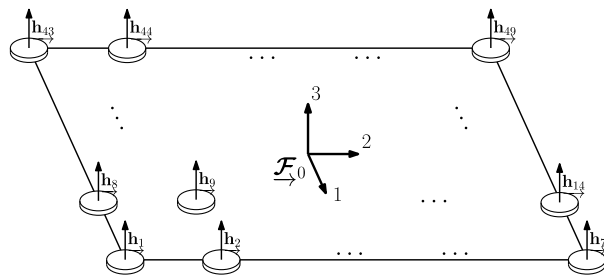
Thus, the optimization problem considered here can be stated as

$$\min_{\mathbf{s}} J(\mathbf{h}), \quad \mathbf{s} = \{\mathbf{h} | \mathbf{h} \in \mathbb{R}^N, \bar{c}(\mathbf{h}) = 0\} \quad (34)$$

### C. Implementation

The problem posed in Eq. (34) is difficult to solve analytically because of its dependency on the solution to the Riccati equation. For this reason, nonlinear numerical techniques are employed. This analysis applies an interior-point algorithm using the `fmincon` function in the MATLAB environment. First, consider the case of a free-free beam. It is discretized using 20 basis functions in a Ritz expansion. The basis functions include the two rigid rotations, the first nine free-free elastic modes in the two axis, and the first nine free-free elastic modes in the three axis. The properties of the beam are presented in Table 1.

The beam is outfitted with 20 CMGs distributed evenly from one end to the other end with a separation distance of  $l/19$ . The stored

**a) Beam****b) Plate****Fig. 3** CMG placement.**Table 2** Plate properties

Property	Symbol	Value
Plate length	$a$	12.5 km
Plate width	$b$	5 km
Mass per area	$\sigma$	0.2662 kg/m <sup>2</sup>
Modulus of rigidity	$D$	$20 \times 10^8 \text{ N}$
Poisson's ratio	$\nu$	0.3
Proportional damping ratios	$\zeta_\alpha$	0.01
Rigid rotation penalization, Eq. (33)	$q$	$1 \times 10^{-4}$

angular momentum of each CMG is nominally parallel to the spanwise direction. This configuration is illustrated in Fig. 3a.

Because gradient-based optimization techniques are used, initial conditions are required. These techniques only ensure a local minimum is reached, and so the optimization is performed using seven different initial conditions and the best results are presented. The following initial conditions are considered: a uniform distribution with

$$h_{s,i} = \frac{1}{c\sqrt{N}}, \quad i = 1, \dots, N \quad (35)$$

and distributions based on sinusoidal functions with

$$h_{s,i} = \frac{1}{C} \int_{a_i}^{b_i} \sin\left(\frac{m\pi x}{l}\right) dx \quad (36)$$

$$\text{or } h_{s,i} = \frac{1}{C} \int_{a_i}^{b_i} \cos\left(\frac{m\pi x}{l}\right) dx \quad (37)$$

where

$$a_i = x_i + \frac{l}{2} - \frac{l}{2N}, \quad b_i = x_i + \frac{l}{2} + \frac{l}{2N}$$

$C$  is chosen to satisfy the constraint  $\mathbf{h}^T \mathbf{h} = c^2$ , and  $m = 1, 2, 3$ .

The plate case is modeled using the finite element method. For the optimization, a uniform  $16 \times 16$  element model is composed using a 16-degree-of-freedom rectangular plate element as described by Zienkiewicz and Taylor [22]. The first 49 modes of this model are retained and used as basis functions in a Ritz expansion. These modes include the two rigid-body rotation modes. The properties of the plate are taken from the Purdue model presented in [23]. The Purdue model is a plate structure with a rigid hub at the center. For this analysis, the rigid mass at the center of the plate in the Purdue model is omitted. The plate properties are given in Table 2.

The plate is outfitted with  $N = 49$  CMGs. These CMGs are distributed in a  $N_x \times N_y$  grid with  $N_x = N_y = 7$ . The spin axes of the CMGs' flywheels are nominally perpendicular to the plate. This configuration is illustrated in Fig. 3b. The optimization is performed using 10 different initial conditions and the best results are presented.

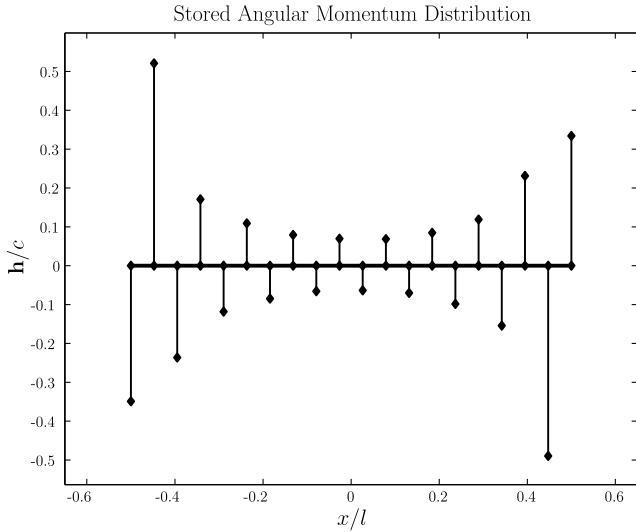


Fig. 4 Optimized CMG distribution for beam.

The following initial conditions are considered: a uniform distribution with

$$h_{s,i} = \frac{1}{c\sqrt{N}}, \quad i = 1, \dots, N \quad (38)$$

a corner distribution evenly lumping all of the stored angular momentum at the plate's corners with

$$\begin{cases} h_{s,i} = \frac{1}{c\sqrt{4}}, & i = \{1, 7, 43, 49\} \\ h_{s,i} = 0, & \text{otherwise} \end{cases} \quad (39)$$

and distributions based on sinusoidal functions with

$$h_{s,i} = \frac{1}{C} \int_{c_i}^{d_i} \int_{a_i}^{b_i} \sin\left(\frac{m\pi x}{a}\right) \sin\left(\frac{n\pi y}{b}\right) dx dy \quad (40)$$

$$\text{or } h_{s,i} = \frac{1}{C} \int_{c_i}^{d_i} \int_{a_i}^{b_i} \cos\left(\frac{m\pi x}{l}\right) \cos\left(\frac{n\pi y}{b}\right) dx dy \quad (41)$$

where

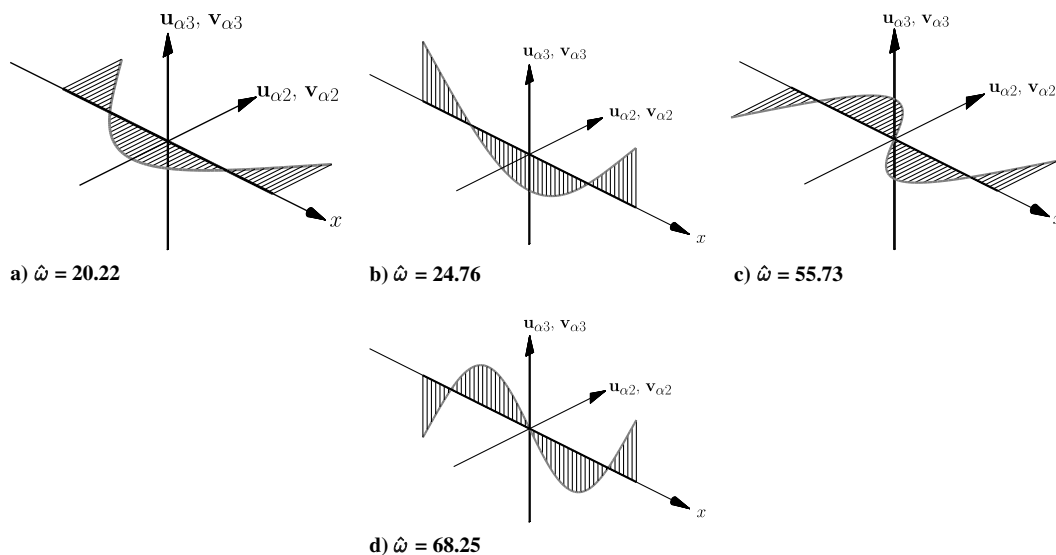


Fig. 5 Elastic modes.

$$\begin{aligned} a_i &= x_i + \frac{a}{2} - \frac{a}{2N_x}, & b_i &= x_i + \frac{a}{2} + \frac{a}{2N_x}, \\ c_i &= y_i + \frac{b}{2} - \frac{b}{2N_y}, & d_i &= y_i + \frac{b}{2} + \frac{b}{2N_y} \end{aligned}$$

$C$  is chosen to satisfy the constraint  $\mathbf{h}^T \mathbf{h} = c^2$ ,  $m = 1, 2$ , and  $n = 1, 2$ .

**D. Optimization Results**

For the free beam, consider the case where  $\hat{c} = c/\sqrt{\rho B l^2} = 1.0$  and  $r = 200$ , where  $B = \sqrt{B_2 B_3}$ . Using the method discussed, the resulting distribution of stored angular momentum with the lowest cost is shown in Fig. 4. One curious result of this optimized distribution is that adjacent gyros have their nominal stored angular momentum in opposite directions, which is consistent with the continuum analysis of the preceding section. To search for an explanation as to why this results in a lower cost, it may be instructive to compare its gyroelastic modes with the elastic modes of a purely elastic beam and the gyroelastic modes of a beam with a single gyro with all of the stored angular momentum lumped at the end of the beam. These modes are illustrated in Figs. 5–7. For the beam with the single gyro, the amount of stored angular momentum is also constrained to have  $\hat{c} = 1.0$ .

The motions of a gyroelastic mode  $\alpha$  are described by

$$\mathbf{q}_\alpha = \mathbf{u}_\alpha \cos(\omega_\alpha t) - \mathbf{v}_\alpha \sin(\omega_\alpha t)$$

where  $\mathbf{u}_\alpha$  and  $\mathbf{v}_\alpha$  now represent the discrete parameter representation of the mode shapes. In Figs. 6 and 7, the mode shape for  $\mathbf{u}_\alpha$  is visualized by the thick black line with many thin lines connecting it to the one axis, and  $\mathbf{v}_\alpha$  is visualized by the thick gray line. The circles and ellipses planar to the one axis show the evolution of the gyroelastic mode through a full period according to the gyroelastic frequency  $\omega$ . The frequencies presented in the figure are scaled according to  $\hat{\omega}_\alpha = \omega_\alpha \sqrt{\rho l^4 / B}$ .

Comparing the elastic modes to the gyroelastic modes for a CMG at  $x = l/2$  illustrates the effect that a concentrated amount of stored angular momentum can have on the gyroelastic modes of the system. It is apparent that having the CMG at the end of the beam flattens out the gyroelastic mode shapes at the end of the beam for both  $\mathbf{u}_\alpha$  and  $\mathbf{v}_\alpha$ . This makes the gyroelastic modes less controllable from that position. It is possible that this is due to the resistance of bodies with large amounts of stored angular momentum to change its axis of rotation.

Now consider the optimized distribution. The staggered directionality of the nominal stored angular momentum of the CMGs

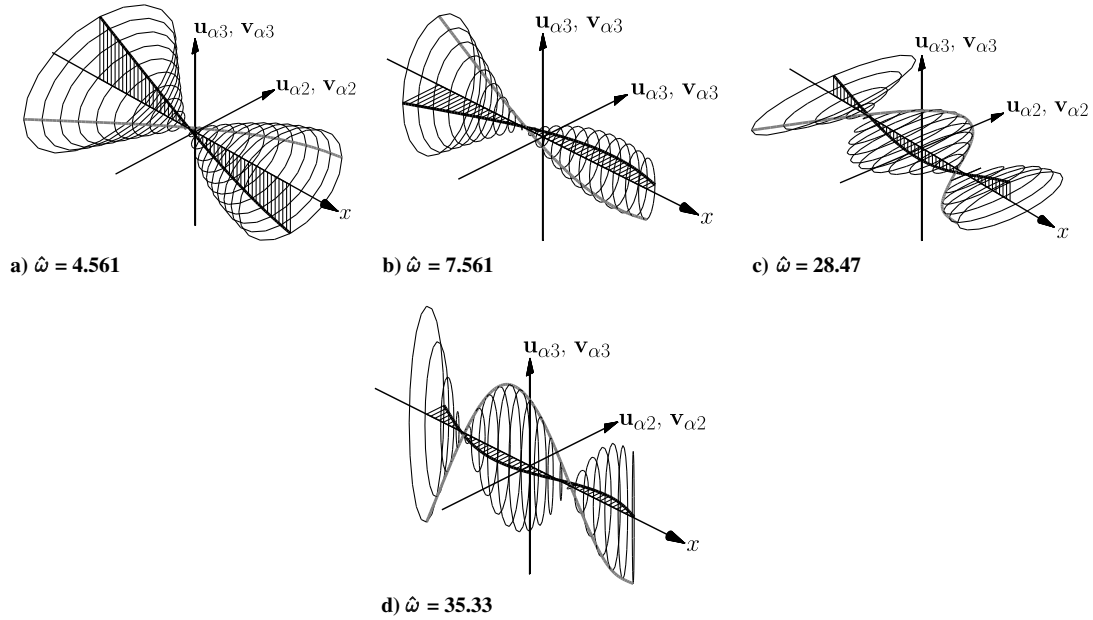


Fig. 6 Gyroelastic modes for single CMG.

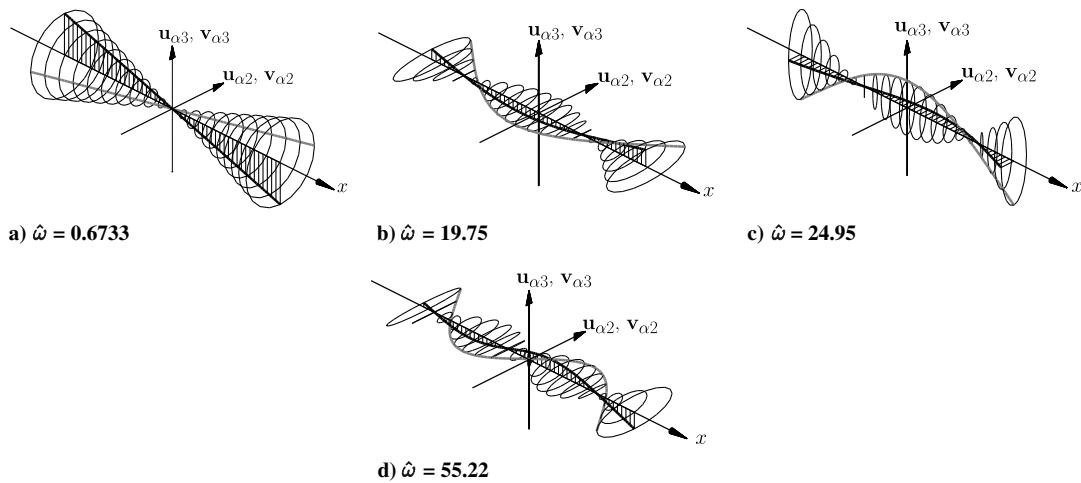


Fig. 7 Gyroelastic modes for optimized distribution.

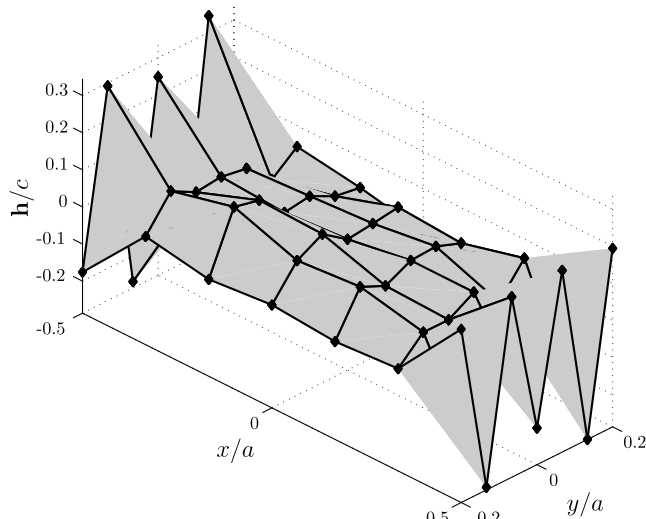


Fig. 8 Optimized CMG distribution for plate.

lowers the total angular momentum of the system, which introduces a rigid precessional mode with low frequency shown in Fig. 7a. It also counters the flattening effect of the gyroelastic modes seen in the single CMG case so that the gyroelastic modes for the optimized case are closer to the elastic modes in both shape and frequency.

Results similar to the free beam case are found for the free plate case. Consider the case in which  $\hat{c} = c/\sqrt{D\sigma a^4} = 1.0$  and  $r = 10$ . The resulting optimized distribution with the lowest cost is shown in Fig. 8. On the short edges of the plate, a staggering of the direction of the nominal stored angular momentum of the CMGs is seen. Concentrating all of the stored angular momentum in a single CMG at the corner  $x = a/2, y = b/2$  results in a flattening of the gyroelastic modes of the plate at the position of the CMG, as shown through the comparison of the elastic modes in Fig. 9 with the gyroelastic modes in Fig. 10. The gyroelastic modes of the optimized distribution do recover the elastic mode shapes for lower frequency modes, as seen in Figs. 11a and 11b. However, they are coupled and their frequencies are different. This correspondence is lost for higher frequencies, as evidenced in Fig. 11c.

### E. System Response

Consider the closed-loop response of the gyroelastic beam system when it is initially deformed and at rest in the shape of a parabola in the three axis. The parabola is described by the function



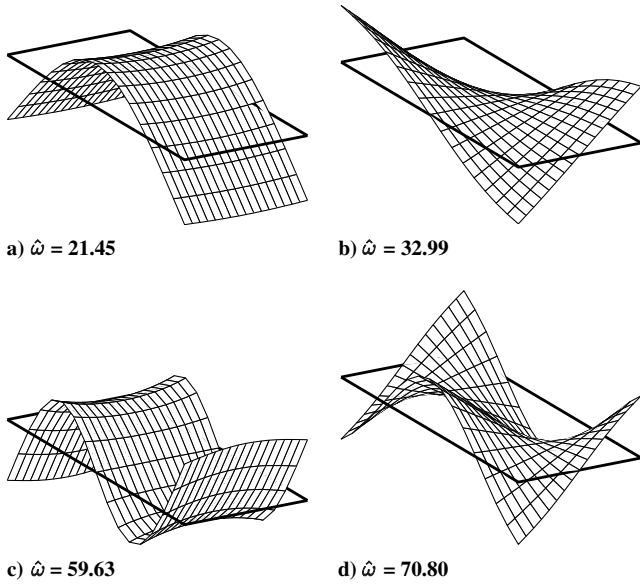


Fig. 9 Free plate elastic modes.

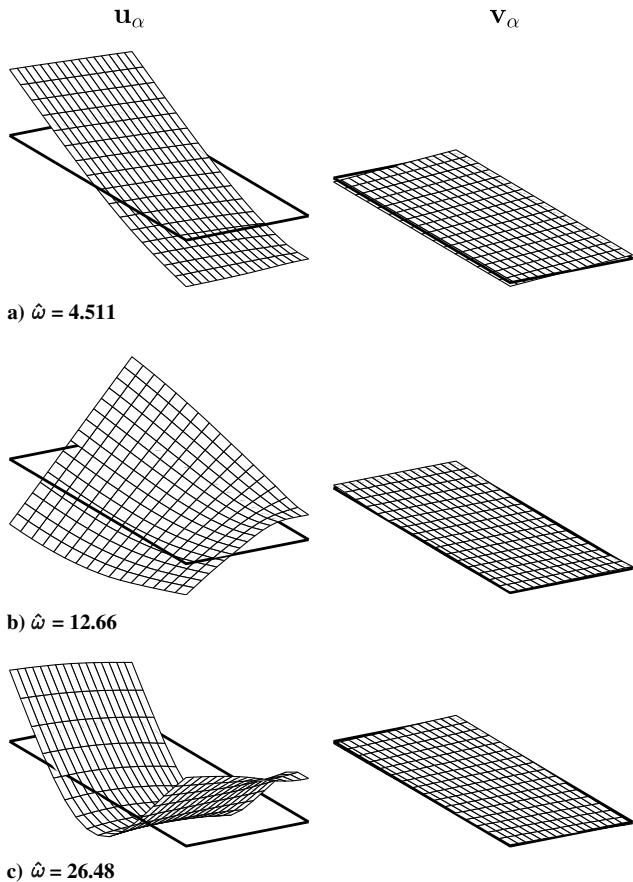


Fig. 10 Free plate single CMG gyroelastic modes ( $\hat{c} = 1.0$ ).

$$z = \frac{1}{25l}x^2$$

Thus, the ends of the beam are deformed 100th of the span of the beam with respect to the beam's center. The response of the system to this initial condition will form a basis for comparison between different distributions of stored angular momentum. For this comparison, the distributions considered include the optimized distribution, a distribution with the stored angular momentum spread uniformly between all 20 gyros as given by Eq. (35), and a

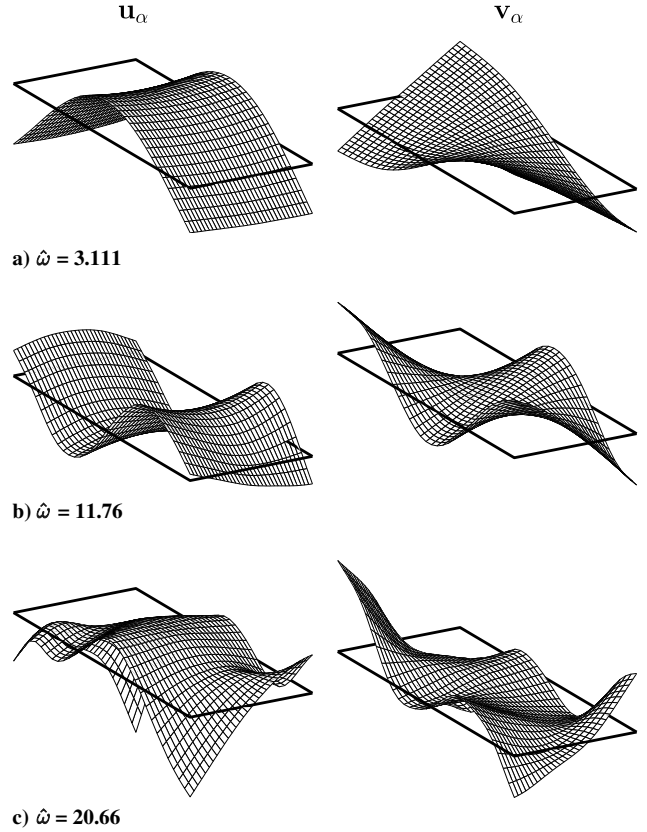


Fig. 11 Free plate CMG distribution gyroelastic modes ( $\hat{c} = 1.0$ ).

distribution with the stored angular momentum lumped evenly between two gyros at the beam ends.

It should be noted that, because the initial conditions involve a symmetric deformation in the three axis, modes corresponding to mode shapes in the two axis and asymmetric mode shapes in the three axis have zero valued initial conditions. To make a quantitative comparison, consider the settling times  $t_s$  for the elastic mode whose mode shape is illustrated in Fig. 5b. The settling time is the time it takes for this mode to reach and stay within 1% of the target values as compared with its initial conditions. This mode is considered because it has nonzero initial conditions, and its settling times are presented in Table 3. The settling time of the optimized distribution for this mode is 11% of the settling time for the uniform distribution and 23% of the settling time for the ends distribution. This shows that the optimization yields significant reduction in settling times in suppressing the vibrations of this system. Starting with the objective function of the LQR problem given in Eq. (32), the optimization of the CMG distribution treated  $\mathbf{x}_0$  as a random variable. This led to taking  $J = \text{tr}(\mathbf{P})$ . However, now that an initial condition is considered, the norm  $\mathbf{x}_0^T \mathbf{P} \mathbf{x}_0$  gives a direct measure of how well each case performs according to the weighting of state and control effort used for the optimization of the stored angular momentum distribution. These values and  $J$  are included in Table 3. This norm yields little insight, however, because the weighting between the states and the control effort was arbitrarily determined to place the closed-loop eigenvalues. To estimate the portion of this norm allocated to the energy of the states and the control effort used to suppress the vibrations of the system, the norms

Table 3 Initial deformation beam performance for  $\hat{c} = 1.0$

Distribution	$t_s, s$	$J$	$\mathbf{x}_0^T \mathbf{P} \mathbf{x}_0$	$J_x$	$J_u$
Optimum	0.57	$2.69 \times 10^5$	$1.49 \times 10^4$	$8.31 \times 10^3$	$6.55 \times 10^3$
Uniform	5.27	$1.77 \times 10^6$	$1.48 \times 10^5$	$7.43 \times 10^4$	$7.41 \times 10^4$
End	2.45	$1.36 \times 10^6$	$7.55 \times 10^4$	$3.76 \times 10^4$	$3.78 \times 10^4$

**Table 4** Initial deformation plate performance for  $\hat{c} = 1.0$ 

Distribution	$t_s, s$	$J$	$\mathbf{x}_0^T \mathbf{P} \mathbf{x}_0$	$J_x$	$J_u$
Optimum	9,048	5,303	$6.43 \times 10^9$	$3.45 \times 10^9$	$2.98 \times 10^9$
Uniform	55,720	12,099	$5.06 \times 10^{10}$	$2.56 \times 10^{10}$	$2.50 \times 10^{10}$
Corner	21,680	32,282	$2.41 \times 10^{10}$	$1.25 \times 10^{10}$	$1.16 \times 10^{10}$

$$J_x = \int_0^\tau \mathbf{x}^T \mathbf{Q} \mathbf{x} dt \quad \text{and} \quad J_u = \int_0^\tau \mathbf{u}^T \mathbf{R} \mathbf{u} dt$$

are calculated for  $\tau$  equal to the settling time for the aforementioned elastic mode. These values are also included in Table 3. From these norms, it can be seen that the optimized distribution outperforms the uniform distribution and the end distribution in both reducing the energy of the states and exerting less control effort.

The closed-loop response of the plate with a parabolic elastic initial deformation while at rest is also considered. The deformation is described by the equation

$$z = \frac{1}{25a} x^2$$

The deformations of the plate at  $x = a/2$  and  $x = -a/2$  are  $a/100$ . The response of the optimized distribution to this deformation is compared with the responses of the uniform distribution from Eq. (38) and the corner distribution from Eq. (39).

As with the beam case, it can be seen that the optimized distribution damps out the vibrations of the plate in less time than the other distributions. The parabolic initial condition is closest in shape to the mode illustrated in Fig. 9a; hence, consider the settling time for this mode shown in Table 4. The optimized distribution has a settling time for this mode that is 16% of the settling time of the uniform distribution and 42% of the settling time of the corner distribution.

To compare the performance of the distributions with respect to dissipating the energy of the states and the control effort exerted, the norms  $\mathbf{x}_0^T \mathbf{P} \mathbf{x}_0$ ,  $J_x$ , and  $J_u$  are considered as defined in the beam case. The time over which the integration is taken is the settling time for the aforementioned mode. The values of these norms are included in Table 4. These values show that the optimized distribution outperforms the uniform distribution and the corner distribution in both damping out the energy of the states and reducing the control effort exerted.

It is important to remember, however, that the results are sensitive to the way in which the objective function is formulated. Optimization tools can only ensure that a series of variables minimizes or maximizes an objective function. The results from the use of these tools are optimal according to the metric by which they were optimized and only provide a means to manage design objectives. To obtain a useful result, one must ensure that the constraints and objective function properly reflect the design requirements when optimization is used in a design process.

## V. Conclusions

This paper has considered the problem of optimizing the location of DGCMGs on a flexible structure for the primary purpose of vibration control. A continuum formulation was proposed, which treated the CMGs as a continuous distribution of stored angular momentum (the gyricity distribution) with an associated distribution of gimbal angles. A discrete parameter approach was also taken for beam and plate models containing a fixed number of DGCMGs at uniformly spaced locations. For both the continuum and discrete parameter approaches, the performance index, which had been optimized with respect to gimbal motion for a given distribution of DGCMGs, was then minimized with respect to the CMGs gyricity distribution. The continuum and discrete parameter results suggest that DGCMGs located for optimal vibration suppression should be implemented so as to avoid contributing stored angular momentum bias over finite regions of the structure. In particular, many small CMGs with alternating signs of the stored angular momentum are superior to a single large CMG.

## Appendix: Comparison Result for Gyricity Distribution

The following development has borrowed from the work in [A1], which considered the sensor location problem for distributed parameter systems. The differences  $\gamma$  and  $\delta$  defined in Eqs. (14) and (15) satisfy the following equations:

$$\begin{aligned} \mathcal{E}\dot{\gamma} + \mathcal{T}(\mathbf{h}_s^*)\gamma + \mathcal{W}(\mathbf{h}_s)\delta &= [\mathcal{W}(\mathbf{h}_s) - \mathcal{W}(\mathbf{h}_s^*)]\xi(\mathbf{h}_s^*) - \delta\mathcal{T}\chi(\mathbf{h}_s), \\ \gamma_0 &= 0 \quad -\mathcal{E}\dot{\delta} + \mathcal{T}^*(\mathbf{h}_s^*)\delta = \mathcal{Q}\gamma - \delta\mathcal{T}^*\xi(\mathbf{h}_s), \quad \delta_T = 0 \end{aligned}$$

Making considerable use of the preceding expressions as well as Eqs. (8–13), produces the following development:

$$\begin{aligned} & \int_0^T \langle \xi(\mathbf{h}_s^*), [\mathcal{W}(\mathbf{h}_s) - \mathcal{W}(\mathbf{h}_s^*)]\xi(\mathbf{h}_s^*) \rangle dt - \int_0^T \langle \xi(\mathbf{h}_s^*), \delta\mathcal{T}\chi(\mathbf{h}_s) \rangle dt \\ &= \int_0^T \langle \xi(\mathbf{h}_s^*), \mathcal{E}\dot{\gamma} + \mathcal{T}(\mathbf{h}_s^*)\gamma + \mathcal{W}(\mathbf{h}_s)\delta \rangle dt \\ &= \int_0^T \langle \xi(\mathbf{h}_s^*), \mathcal{W}(\mathbf{h}_s)\delta \rangle dt + \int_0^T \langle \xi(\mathbf{h}_s^*), \mathcal{E}\dot{\gamma} + \mathcal{T}(\mathbf{h}_s^*)\gamma \rangle dt \\ &= \int_0^T \langle \xi(\mathbf{h}_s^*), \mathcal{W}(\mathbf{h}_s)\delta \rangle dt \\ & \quad + \int_0^T \langle -\mathcal{E}\dot{\xi}(\mathbf{h}_s^*) + \mathcal{T}^*(\mathbf{h}_s^*)\xi(\mathbf{h}_s^*), \gamma \rangle dt + [\langle \xi(\mathbf{h}_s^*), \mathcal{E}\gamma \rangle]_{t=0}^T \\ &= \int_0^T \langle \xi(\mathbf{h}_s^*), \mathcal{W}(\mathbf{h}_s)\delta \rangle dt + \int_0^T \langle \chi(\mathbf{h}_s^*), \mathcal{Q}\gamma \rangle dt \\ &= \int_0^T \langle \xi(\mathbf{h}_s^*), \mathcal{W}(\mathbf{h}_s)\delta \rangle dt + \int_0^T \langle -\mathcal{E}\dot{\delta} + \mathcal{T}^*(\mathbf{h}_s^*)\delta, \chi(\mathbf{h}_s^*) \rangle dt \\ & \quad + \int_0^T \langle \chi(\mathbf{h}_s^*), \delta\mathcal{T}^*\xi(\mathbf{h}_s) \rangle dt \\ &= \int_0^T \langle \xi(\mathbf{h}_s^*), \mathcal{W}(\mathbf{h}_s)\delta \rangle dt \\ & \quad + \int_0^T \langle \mathcal{E}\dot{\chi}(\mathbf{h}_s^*) + \mathcal{T}(\mathbf{h}_s^*)\chi(\mathbf{h}_s^*), \delta \rangle dt - [\langle \mathcal{E}\chi(\mathbf{h}_s^*), \delta \rangle]_{t=0}^T \\ & \quad + \int_0^T \langle \chi(\mathbf{h}_s^*), \delta\mathcal{T}^*\xi(\mathbf{h}_s) \rangle dt \\ &= \int_0^T \langle \xi(\mathbf{h}_s^*), \mathcal{W}(\mathbf{h}_s)\delta \rangle dt - \int_0^T \langle \mathcal{W}(\mathbf{h}_s^*)\xi(\mathbf{h}_s^*), \delta \rangle dt + \langle \mathcal{E}\chi_0, \delta_0 \rangle \\ & \quad + \int_0^T \langle \chi(\mathbf{h}_s^*), \delta\mathcal{T}^*\xi(\mathbf{h}_s) \rangle dt \\ &= \int_0^T \langle \xi(\mathbf{h}_s^*), [\mathcal{W}(\mathbf{h}_s) - \mathcal{W}(\mathbf{h}_s^*)]\delta \rangle dt \\ & \quad + \langle \mathcal{E}\chi_0, [\mathcal{P}(\mathbf{h}_s^*)|_{t=0} - \mathcal{P}(\mathbf{h}_s)|_{t=0}]\mathcal{E}\chi_0 \rangle \\ & \quad + \int_0^T \langle \chi(\mathbf{h}_s^*), \delta\mathcal{T}^*\xi(\mathbf{h}_s) \rangle dt \\ &= \int_0^T \langle \xi(\mathbf{h}_s^*), [\mathcal{W}(\mathbf{h}_s) - \mathcal{W}(\mathbf{h}_s^*)]\delta \rangle dt + 2(\mathcal{J}(\mathbf{h}_s^*) - \mathcal{J}(\mathbf{h}_s)) \\ & \quad + \int_0^T \langle \chi(\mathbf{h}_s^*), \delta\mathcal{T}^*\xi(\mathbf{h}_s) \rangle dt \end{aligned}$$

The last equality can be rearranged to give

$$\begin{aligned} \mathcal{J}(\mathbf{h}_s) - \mathcal{J}(\mathbf{h}_s^*) &= \frac{1}{2} \int_0^T \langle \xi(\mathbf{h}_s^*), [\mathcal{W}(\mathbf{h}_s^*) - \mathcal{W}(\mathbf{h}_s)]\xi(\mathbf{h}_s^*) \rangle dt \\ & \quad + \frac{1}{2} \int_0^T \langle \xi(\mathbf{h}_s^*), [\mathcal{W}(\mathbf{h}_s) - \mathcal{W}(\mathbf{h}_s^*)]\delta \rangle dt \\ & \quad + \frac{1}{2} \int_0^T \langle \xi(\mathbf{h}_s^*), \delta\mathcal{T}\chi(\mathbf{h}_s) \rangle dt + \frac{1}{2} \int_0^T \langle \chi(\mathbf{h}_s^*), \delta\mathcal{T}^*\xi(\mathbf{h}_s) \rangle dt \quad (\text{A1}) \end{aligned}$$

Also, the use of Eqs. (14) and (15) yields the system of equalities

$$\begin{aligned}
& \int_0^T \langle \xi(\mathbf{h}_s^*), [\mathcal{W}(\mathbf{h}_s) - \mathcal{W}(\mathbf{h}_s^*)] \delta \rangle dt - \int_0^T \langle \delta, \delta \mathcal{T} \chi(\mathbf{h}_s) \rangle dt \\
&= \int_0^T \langle \delta, \mathcal{E} \dot{\gamma} + \mathcal{T}(\mathbf{h}_s^*) \gamma + \mathcal{W}(\mathbf{h}_s) \delta \rangle dt \\
&= \int_0^T \langle \delta, \mathcal{W}(\mathbf{h}_s) \delta \rangle dt + \int_0^T \langle \delta, \mathcal{E} \dot{\gamma} + \mathcal{T}(\mathbf{h}_s^*) \gamma \rangle dt \\
&= \int_0^T \langle \delta, \mathcal{W}(\mathbf{h}_s) \delta \rangle dt + \int_0^T \langle \gamma, -\mathcal{E} \dot{\delta} + \mathcal{T}^*(\mathbf{h}_s^*) \delta \rangle dt + [\langle \delta, \mathcal{E} \gamma \rangle]_{t=0}^T \\
&= \int_0^T \langle \delta, \mathcal{W}(\mathbf{h}_s) \delta \rangle dt + \int_0^T \langle \gamma, \mathcal{Q} \gamma \rangle dt - \int_0^T \langle \gamma, \delta \mathcal{T}^* \xi(\mathbf{h}_s) \rangle dt
\end{aligned}$$

Noting the definitions of  $\delta$  and  $\gamma$ , the last equality is equivalent to

$$\begin{aligned}
& \frac{1}{2} \int_0^T \langle \xi(\mathbf{h}_s^*), [\mathcal{W}(\mathbf{h}_s) - \mathcal{W}(\mathbf{h}_s^*)] \delta \rangle dt \\
&= \frac{1}{2} \int_0^T \langle \delta, \mathcal{W}(\mathbf{h}_s) \delta \rangle dt + \frac{1}{2} \int_0^T \langle \gamma, \mathcal{Q} \gamma \rangle dt \\
&\quad + \frac{1}{2} \int_0^T \langle \xi(\mathbf{h}_s^*), \delta \mathcal{T} \chi(\mathbf{h}_s) \rangle dt \\
&\quad - \frac{1}{2} \int_0^T \langle \chi(\mathbf{h}_s^*), \delta \mathcal{T}^* \xi(\mathbf{h}_s) \rangle dt \tag{A2}
\end{aligned}$$

Combining Eqs. (A1) and (A2) gives

$$\begin{aligned}
\mathcal{J}(\mathbf{h}_s) - \mathcal{J}(\mathbf{h}_s^*) &= \frac{1}{2} \int_0^T \langle \xi(\mathbf{h}_s^*), [\mathcal{W}(\mathbf{h}_s^*) - \mathcal{W}(\mathbf{h}_s)] \xi(\mathbf{h}_s^*) \rangle dt \\
&\quad + \int_0^T \langle \xi(\mathbf{h}_s^*), \delta \mathcal{T} \chi(\mathbf{h}_s) \rangle dt + \frac{1}{2} \int_0^T [\langle \delta, \mathcal{W}(\mathbf{h}_s) \delta \rangle + \langle \gamma, \mathcal{Q} \gamma \rangle] dt \tag{A3}
\end{aligned}$$

which is the desired result.

- [A1] Bensoussan, A., "Optimization of Sensors' Location in a Distributed Filtering Problem," *Stability of Stochastic Dynamical Systems*, Vol. 294, Lecture Notes in Mathematics, Springer-Verlag, Berlin, 1972, pp. 62–84.

## References

- [1] Aubrun, J. N., and Margulies, G., "Gyrodampers for Large Space Structures," NASA CR-159171, Feb. 1979.
- [2] Brown, D., and Peck, M., "Scissored-Pair Control Moment Gyros: A Mechanical Constraint Saves Power," *Journal of Guidance, Control, and Dynamics*, Vol. 31, No. 6, 2008, pp. 1823–1826. doi:10.2514/1.37723
- [3] Shi, J.-F., and Damaren, C. J., "Control Law for Active Structural Damping Using a Control Moment Gyro," *Journal of Guidance, Control, and Dynamics*, Vol. 28, No. 3, 2005, pp. 550–553. doi:10.2514/1.11269
- [4] Muise, A., and Bauer, R. J., "Comparison of the Effectiveness of Double- vs. Single-Gimbaled Control Moment Gyros for Vibration Suppression," *Transactions of the Canadian Society of Mechanical Engineering*, Vol. 29, No. 3, 2005, pp. 389–402.
- [5] Hu, Q., Jia, Y., and Xu, S., "Simple Adaptive Control for Vibration Suppression of Space Structures Using Control Moment Gyros," AIAA Paper 2013-4871, Aug. 2013.
- [6] Yang, L.-F., Mikulas, M. M., Park, K. C., and Su, R., "Slewing Maneuvers and Vibration Control of Space Structures by Feedforward/Feedback Moment-Gyro Controls," *Journal of Dynamic Systems, Measurement and Control*, Vol. 117, No. 3, 1995, pp. 343–351. doi:10.1115/1.2799125
- [7] D'Eleuterio, G. M. T., and Hughes, P. C., "Dynamics of Gyroelastic Continua," *Journal of Applied Mechanics*, Vol. 51, No. 2, 1984, pp. 415–422. doi:10.1115/1.3167634
- [8] D'Eleuterio, G. M. T., and Hughes, P. C., "Dynamics of Gyroelastic Spacecraft," *Journal of Guidance, Control, and Dynamics*, Vol. 10, No. 4, 1987, pp. 401–405. doi:10.2514/3.20231
- [9] Damaren, C. J., and D'Eleuterio, G. M. T., "Optimal Control of Large Space Structures Using Distributed Gyricity," *Journal of Guidance, Control, and Dynamics*, Vol. 12, No. 5, 1989, pp. 723–731. doi:10.2514/3.20467
- [10] Damaren, C. J., and D'Eleuterio, G. M. T., "Controllability and Observability of Gyroelastic Vehicles," *Journal of Guidance, Control, and Dynamics*, Vol. 14, No. 5, 1991, pp. 886–894. doi:10.2514/3.20728
- [11] Li, Z., and Bainum, P., "Vibration Control of Flexible Spacecraft Integrating a Momentum Exchange Controller and a Distributed Piezoelectric Actuator," *Journal of Sound and Vibration*, Vol. 177, No. 4, 1994, pp. 539–553. doi:10.1006/jsvi.1994.1450
- [12] Denoyer, K., and Kwak, M., "Dynamic Modelling and Vibration Suppression of a Slewing Structure Utilizing Piezoelectric Sensors and Actuators," *Journal of Sound and Vibration*, Vol. 189, No. 1, 1996, pp. 13–31. doi:10.1006/jsvi.1996.0003
- [13] Damaren, C. J., and Oguamanam, D. C. D., "Vibration Control of Spacecraft Box Structures Using a Collocated Piezo-Actuator/Sensor," *Journal of Intelligent Material Systems and Structures*, Vol. 15, No. 5, 2004, pp. 369–374. doi:10.1177/1045389X04040901
- [14] Hu, Y.-R., and Ng, A., "Active Robust Vibration Control of Flexible Structures," *Journal of Sound and Vibration*, Vol. 288, Nos. 1–2, 2005, pp. 43–56. doi:10.1016/j.jsv.2004.12.015
- [15] Moshrefi-Torbati, M., Keane, A., Elliott, S., Brennan, M., Anthony, D., and Rogers, E., "Active Vibration Control (AVC) of a Satellite Boom Structure Using Optimally Positioned Stacked Piezoelectric Actuators," *Journal of Sound and Vibration*, Vol. 292, Nos. 1–2, 2006, pp. 203–220. doi:10.1016/j.jsv.2005.07.040
- [16] Kamesh, D., Pandiyan, R., and Ghosal, A., "Modeling, Design and Analysis of Low Frequency Platform for Attenuating Micro-Vibration in Spacecraft," *Journal of Sound and Vibration*, Vol. 329, No. 17, 2010, pp. 3431–3450. doi:10.1016/j.jsv.2010.03.008
- [17] Wang, Q., and Wang, C., "Controllability Index for Optimal Design of Piezoelectric Actuators in Vibration Control of Beam Structures," *Journal of Sound and Vibration*, Vol. 242, No. 3, 2001, pp. 507–518. doi:10.1006/jsvi.2000.3357
- [18] Halim, D., and Moheimani, S. O. R., "Optimization Approach to Optimal Placement of Collocated Piezoelectric Actuators and Sensors on a Thin Plate," *Mechatronics*, Vol. 13, No. 1, 2003, pp. 27–47. doi:10.1016/S0957-4158(01)00079-4
- [19] Damaren, C. J., "Optimal Location of Collocated Piezo-Actuator/Sensor Combinations in Spacecraft Box Structures," *Smart Materials and Structures*, Vol. 12, No. 3, 2003, pp. 494–499. doi:10.1088/0964-1726/12/3/321
- [20] Hughes, P. C., and D'Eleuterio, G. M. T., "Modal Parameter Analysis of Gyroelastic Continua," *Journal of Applied Mechanics*, Vol. 53, No. 4, 1986, pp. 918–924. doi:10.1115/1.3171881
- [21] Juang, J.-N., "Optimal Design of a Passive Vibration Absorber for a Truss Beam," *Journal of Guidance, Control, and Dynamics*, Vol. 7, No. 6, 1984, pp. 733–739. doi:10.2514/3.19920
- [22] Zienkiewicz, O. C., and Taylor, R. L., *Finite Element Method*, Vol. 2, Solid Mechanics, 5th ed., Butterworth-Heinemann, Woburn, MA, 2000, pp. 151–153.
- [23] Hablani, H. B., "More Accurate Modeling of the Effects of Actuators in Large Space Structures," *Acta Astronautica*, Vol. 8, No. 4, 1981, pp. 361–376. doi:10.1016/0094-5765(81)90005-9